CHAPTER 5

Experimental Testing and Results

5.1 Introduction

This chapter sets out to verify through experimental testing the Pi-based scaling laws developed for the PR manipulator. The chapter begins by discussing the experimental systems and the overall approach to the testing. A methodology is developed to experimentally verify motor parameters. Experimental results of the controlled model and prototype PR manipulators are presented and analyzed. Finally, a new dimensionless variable is developed to predict the prototype's reference voltage and to explain how Π_4 in (3.69) is of little consequence for this controller and application.

5.2 Model and Prototype Hardware Configurations

The model and prototype PR manipulators developed for testing consisted of two main links. The translational link was connected to a slider mechanism that was actuated by a pulley system connected to a gearmotor. The rotation link was attached by a revolute joint to the end of the translation link. The model system was actuated by a belt and pulley system that was connected to a gearmotor mounted on the translation link. The prototype's rotation link was actuated by a direct gearing system. Position was sensed by potentiometers in both systems, and sensor power was provided by a bipolar 12 volts, 1.5 amps power supply that was isolated from the motors' power electronics. Sensor calibration was performed by reading voltages for corresponding angular and linear displacements and supplying this data to Matlab's polyfit function. The motors operated without tachometers so no direct velocity measurements were taken for the experimentation. Both systems are presented in Figure 5.1. Appendix C lists their link dimensions and their nominal motor parameters.

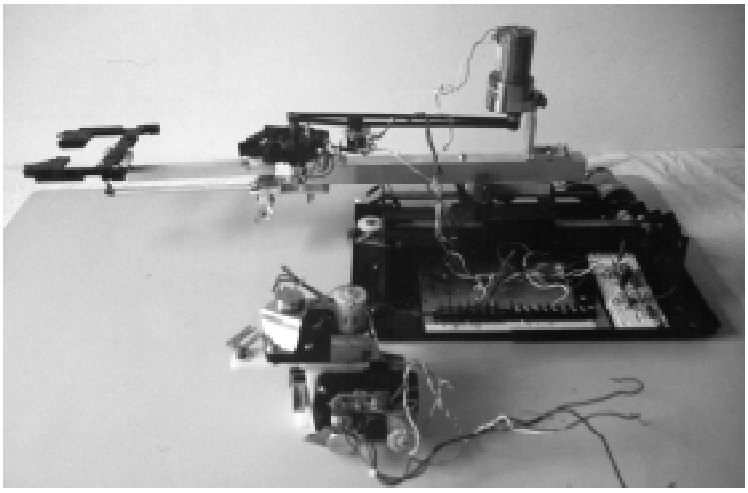

Figure 5.1: Model and prototype PR manipulators

Figure 5.2 shows two more views of the prototype system.

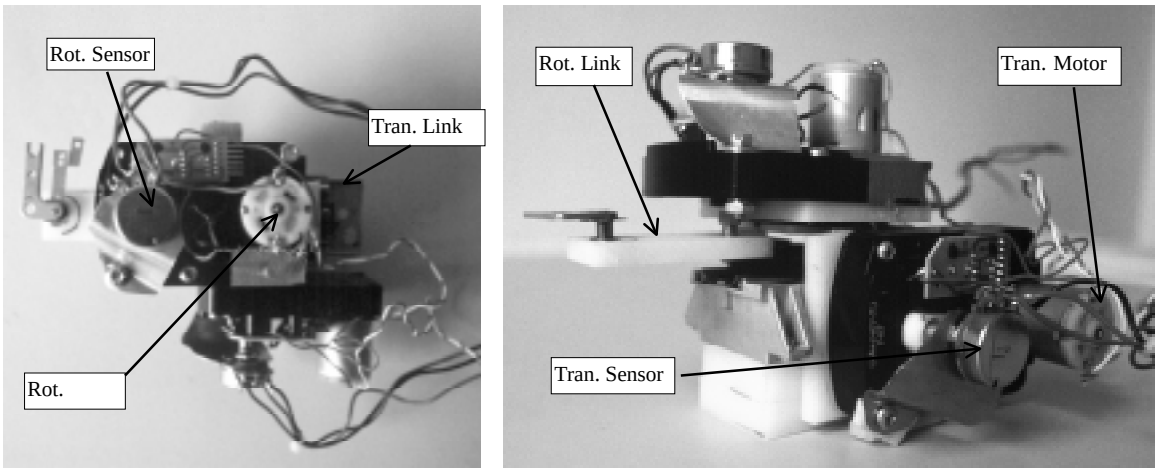

(a) (b)

Figure 5.2: Prototype PR manipulator; (a) top view, (b) three-quarters side view

Figure 5.3 is a one-line drawing of the control and power equipment used for both manipulators. Control was provided by a 486-33 MHz AT class PC equipped with two data acquisition cards. Together, the cards provided sixteen 12-bit analog input channels and two 12-bit analog output channels. All connections were single ended with gains of +/- 5 volts for both the input and output channels. The main control program was written in Borland 3.1 C for DOS and called vendor-provided functions that performed the A/D and D/A conversions. An onboard Intel 8254 interval timer programmed in mode 2 generated a periodic clock that was used to pace the conversions of the input and output signals. The sample rate for the model and prototype testing was set to 100 Hz. To verify the sample rate, a program written in C produced an analog square wave signal of the same period that was paced by the 8254 interval timer. An oscilloscope, connected to the output channel, displayed the square wave and its period. Through this simple test, it was confirmed that this system could produce a steady, repeatable sample rate of 100 Hz.

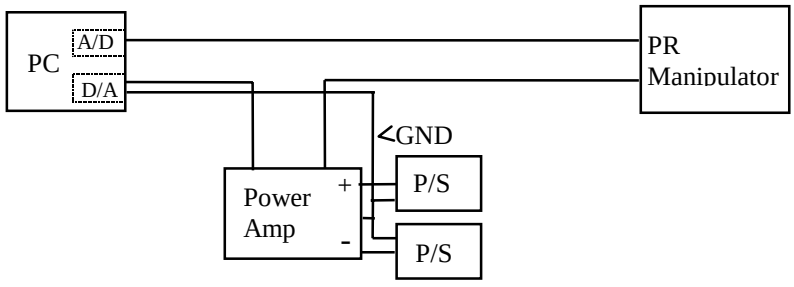

Figure 5.3: One-line drawing of system configuration

A variation on a Darlington amplifier (Hoenig and Payne, 1973) provided power amplification. This voltage source amplifier was tuned to have a gain of 2, and was powered by two unipolar 13.5 volts, 3 amps power supplies. 10 volts was assumed to be the point of amplifier saturation, and thus control references were clamped at this level. To confirm that this design was indeed voltage regulated, a range of power resistors were connected to the amplifier's output terminals. Current and voltage measurements were taken and used in Ohm's law to prove amplifier linearity.

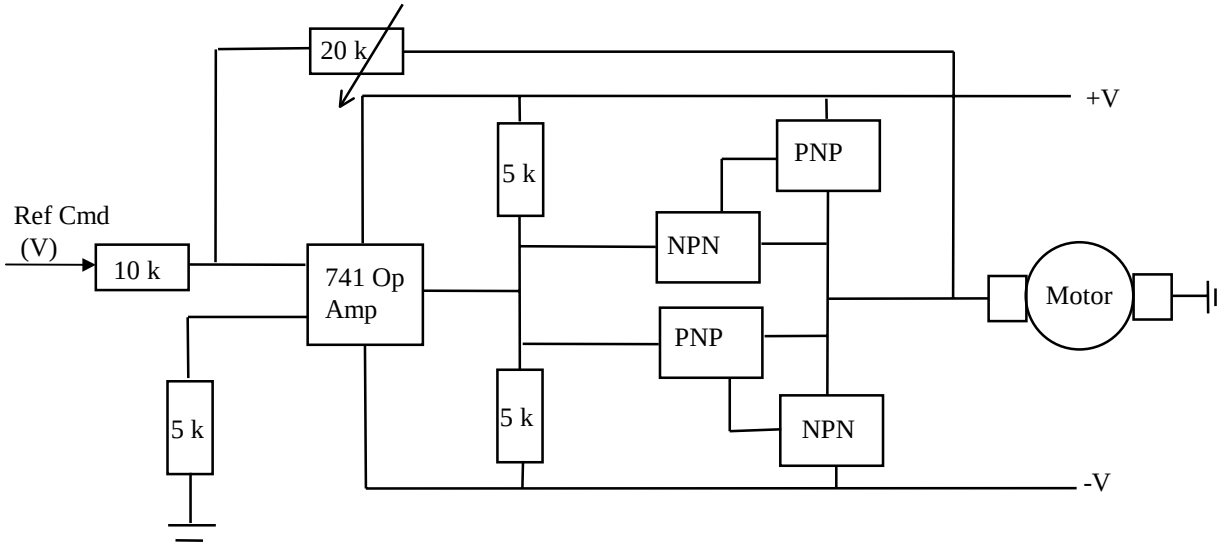

Figure 5.4: Schematic of power amplifier

5.3 Experimental Approach

The model and prototype systems described in section 5.2 were tested using the control code presented in Appendix F. As remarked earlier, the C code mirrors the Matlab code used for Chapter 4's simulations and is located in Appendix E. The purpose of this experimental work was to confirm the theoretical model and simulations presented in Chapter 4, and thus validate the scaling laws derived from the Pi theorem.

The testing proceeded by first identifying the manipulators' motor parameters. The scheme, developed in the next section, compares the experimental position response to a closed form solution modeled in Matlab. Other motor parameters such as inertia and friction torques were identified independently and incorporated in the closed form solution. These techniques are presented in Section 5.4.

After the motor data was collected, the model system was experimentally tested using the trajectory planner and computed torque controller that produced Chapter 4's simulations. The prototype system was similarly tested. For both the prototype and model systems, runs were conducted with the friction compensation turned on and off so that its effectiveness could be

readily observed. All tests were conducted without feedback control. The experimental and the simulated responses were compared for both systems. Evaluation of the responses were performed to determine whether link dynamics had any effect. Finally, an assessment was made from the experimental results on the validity of the Pi-based scaling laws.

5.4 Off-line Motor Parameter Estimation

5.4.1 Introduction

The motor parameters located in tables C2 (a,b) and C4 (a,b) in Appendix C were nominal values supplied by the motor manufacturer. Some of the parameters were averaged from different windings of a given frame size. Error associated with the friction terms are stated to be as high as 50%. Therefore, to have confidence in the experimental testing, it was necessary to develop a motor identification scheme.

Two levels of motor identification were employed for this study. In general, the model system's motor parameters were well identified. This was confirmed by stepping the motor and comparing the experimental response to an analytical one that used the motor parameters in tables C2 (a,b). The static and Coulomb friction terms were manually identified as will be illustrated below. The prototype motor parameters supplied by the manufacture, however, had been generalized for several frame sizes and had key terms omitted. A slightly more involved identification scheme was developed to establish the magnitude of these terms.

Before this discussion begins, recall that in the literature review there were several reports that treated on-line parameter identification. These schemes are mostly concerned with identifying parameters that are subject to change due to fluctuations in temperature and loading. For example, the last link of a multi-revolute joint manipulator could experience normal force load changes at its extended range of operation; changing friction terms. However, for purposes of confirming the Pi scaling laws developed in this thesis, on-line parameter estimation methods are not necessary.

Because the motors used in the experimental testing did not have tachometers, frequency analysis, and the traditional system identifications schemes were not employed. Additionally, measuring a motor's mechanical time constant from a velocity step response was not attempted either. Instead, identification was performed by using the simple technique of stepping the motor and matching experimental and analytical position responses. A *dimensioned* closed form solution was used to confirm key motor parameters. Its derivation was similar to the nondimensional closed form solution developed in Chapter 3 (also used in this analysis).

The derivation of the closed form dimensioned equation begins with:

$$V = \frac{JR}{K_t}\frac{d\theta^2}{dt^2} + \frac{R}{K_t}D_1\frac{d\theta}{dt} + K_b\frac{d\theta}{dt} + \frac{R}{K_t}T_C \qquad (5.1)$$

which is the dimensionally homogeneous equation of the motor derived in section 3.3 with the load and stiction terms set to zero. The goal is to determine J, K_t, K_b, and T_C. Because damping, D_1, is usually small, it is ignored for the moment. Solving equation (5.1) for $\theta(t)$ reveals that only speed ω, Coulomb friction T_C, and a damping constant K_D influence the motor's response after transients have dissipated. Equation (5.1) becomes:

$$\frac{JR}{K_t}\frac{d\theta^2}{dt^2} + K_b\frac{d\theta}{dt} = V - \frac{R}{K_t}T_C$$

$$\frac{d\theta^2}{dt^2} + \frac{K_t K_b}{JR}\frac{d\theta}{dt} = \frac{K_t}{JR}V - \frac{T_C}{J}$$

$$\theta(s)s^2 + \frac{K_t K_b}{JR}\theta(s)s = \frac{K_t}{JR}\frac{V}{s} - \frac{T_C}{Js}$$

$$\theta(s) = \left(\frac{K_t V}{JR} - \frac{T_C}{J}\right)\left(\frac{1}{s^2\left(s + \left(\frac{K_t K_b}{JR}\right)\right)}\right)$$

Taking the inverse Laplace produces:

$$\theta(t) = \left(\frac{K_t V}{JR} - \frac{T_C}{J}\right)\left(\frac{1}{\left(\frac{1}{\frac{K_t K_b}{JR}}\right)^2}\right)\left(e^{-\left(\frac{K_t K_b}{JR}\right)t} + \left(\frac{K_t K_b}{JR}\right)t - 1\right)$$

$$\theta(t) = \left(\frac{V}{K_b} - \left(\frac{R}{K_t K_b}\right)T_C\right)\left(t - \tau_m + \tau_m e^{-\left(\frac{t}{\tau_m}\right)}\right)$$

and with initial conditions added becomes:

$$\theta(t) = \left(\frac{V}{K_b} - \left(\frac{R}{K_t K_b}\right)T_C\right)\left(t - \tau_m + \tau_m e^{-\left(\frac{t}{\tau_m}\right)}\right) + \theta_0 \qquad (5.2)$$

Equation (5.2) is substituted into (5.3) in order to compute a translational displacement.

$$x_{geared} = N_T r\theta(t) \qquad (5.3)$$

In the case of the model system motors, only T_C has a degree of uncertainty. Because of this, it is a simple exercise to step the motor and adjust the Coulomb friction term until the experimental and analytical responses match. Determining the prototype system's motors parameters, however, required a more rigorous method which will be presented later in the chapter.

The *nondimensional* equations developed in Chapter 3 and used in section 4.3 of Chapter 4 are presented again for purposes of determining the effects stiction and damping have on the model and prototype motors' responses.

$$\begin{aligned}\overline{\theta}(\bar{t}) &= (\overline{V} - \overline{T}_s)\left(e^{-(\overline{D}_1+1)\bar{t}} + (\overline{D}_1+1)\bar{t} - 1\right) \\ &+(\overline{T}_s - \overline{T}_C)\left(e^{-(\overline{D}_1+1)(\bar{t}-\bar{t}_s)} + (\overline{D}_1+1)(\bar{t}-\bar{t}_s) - 1\right)\left(u(\bar{t}-\bar{t}_s)\right) + \overline{\theta}_0\end{aligned} \tag{5.4}$$

where

$$u(\bar{t}-\bar{t}_s) = 0 \quad \text{for } \bar{t} < \bar{t}_s$$
$$u(\bar{t}-\bar{t}_s) = 1 \quad \text{for } \bar{t} \geq \bar{t}_s$$

Recall that the following equations are used to dimension equation (5.4)

$$\overline{\theta}_0 = \frac{x_0}{Nr\theta_{ref}} = \frac{x_0}{Nr\omega_{ref}t_{ref}}$$

$$\overline{\theta} = \frac{x}{Nr\theta_{ref}} = \frac{x}{Nr\omega_{ref}t_{ref}} = \frac{xK_b^2K_t}{NrV_{ref}JR}$$

$$\bar{t} = \frac{t}{t_{ref}} = \frac{t}{\tau_m}$$

The dimensionless model stated in (5.4) includes, static, Coulomb, and viscous friction terms and initial conditions. The term t_s is the time value where the system transitions from static to kinetic friction.

The stiction constant, T_s is quite easily determined by measuring current through a quiescent motor while increasing terminal voltage in small step sizes. The current measured just before the motor shaft begins to rotate is called the break-out current, I_s. Stiction is derived by multiplying this term by the torque constant, or:

$$T_s = K_t I_s \tag{5.5}$$

Equations (5.1-5.5) form the basis from which the model and prototype motor parameters were identified. It should be noted that the time constant for the transition from static to kinetic friction was not identified experimentally. Results from the literature were relied upon to size this value (de Witt *et al.*, 1997).

5.4.2 Model System Motor-ID

Figure 5.5 compares the dimensioned response generated from equation (5.4) with an experimental response. Both were given a 9.2 volt step input and were run for 3 seconds to ensure that the responses had reached steady state.

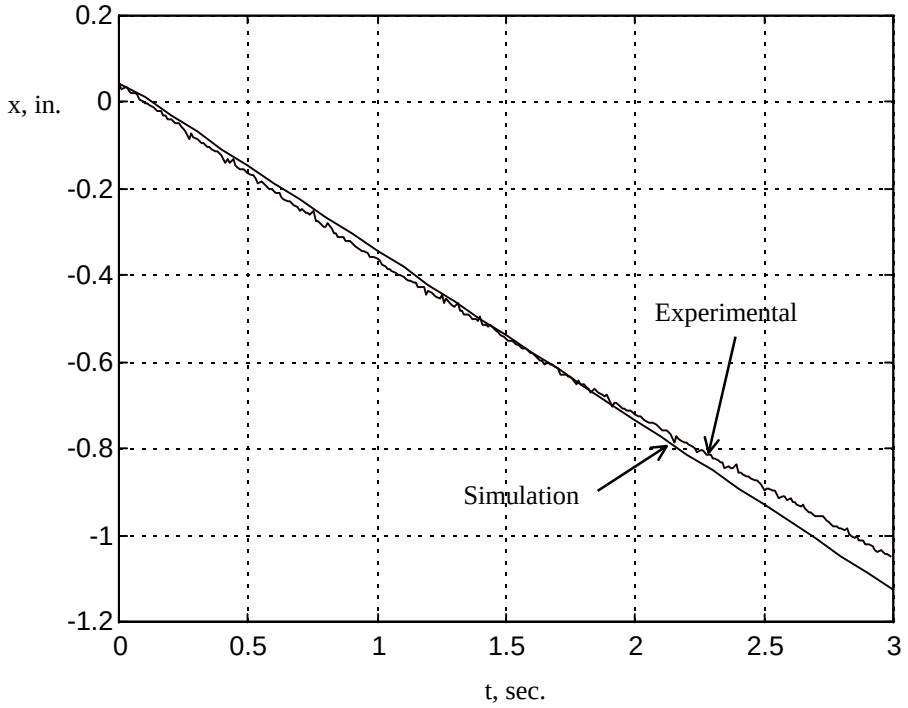

Figure 5.5: Model (translation) motor's experimental position response

The experimental response in Figure 5.5 is for a run where the motor is coupled to the translational load. The simulation response in this figure, however, does not include a load term, and assumes the motor is uncoupled and freely running. Both curves agree because gearing has eliminated link dynamics and inertial effects as claimed earlier in the thesis. A slight disparity between the responses does exist, however, midway into the run. It appears that a low frequency sine function is riding on top of the experimental response. Inspection of the experimental apparatus lead to a conclusion that an out-of-round pulley coincided with this function's period and was the source of the disturbance. It is ignored with little consequence for the rest of the thesis.

Equation (5.4) predicts a transient that is attributable to stiction. Figure 5.6 attempts to illustrate this effect for both the experimental and analytical responses. However, signal noise

makes this analysis difficult to pursue. Furthermore, the large step input minimizes the effect of stiction. Later in this chapter, low velocity testing will more clearly reveal this phenomenon.

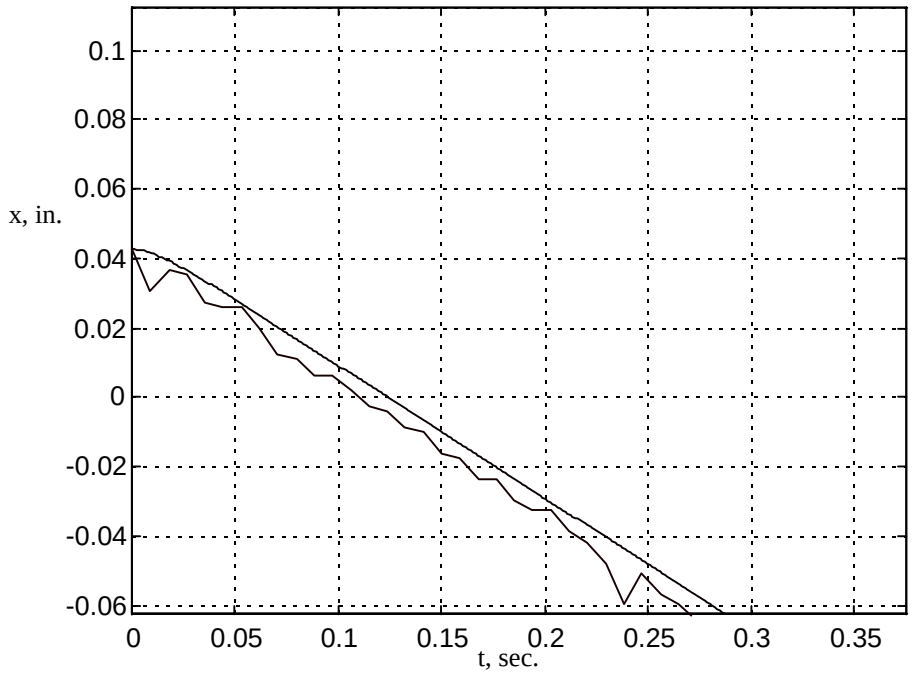

Figure 5.6: Exploded view of the model system's translation step response

Figure 5.7 compares the analytical responses with and without damping and static friction. Notice there are no perceptible differences after steady state has been reached between the responses generated from equations (5.3) and (5.4). This suggests that viscous friction, D_1 for the model motor is theoretically not significant. As mentioned earlier, the motor's speed ω, Coulomb friction, T_C, and damping constant, K_D are the most important parameters that affect a PM d.c. motor's steady state position response.

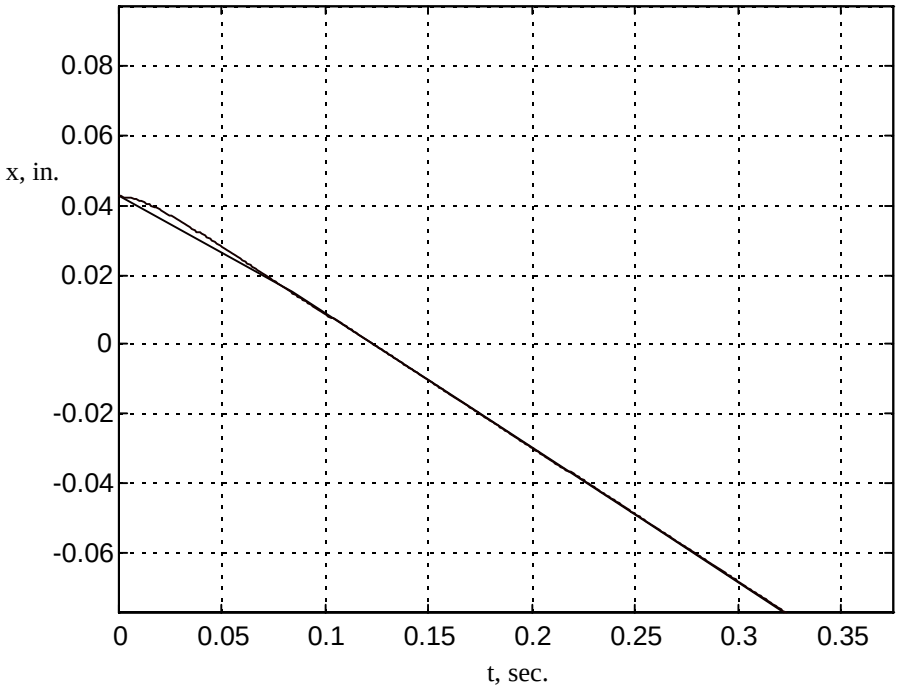

Figure 5.7: Simulated response of Equations (5.3) and (5.4)

Tables 5.1 and 5.2 lists the model system's motor parameters that were experimentally verified using the methods in this section. Inductance was not tested for directly. However, the manufacturer's data suggests that this term has little influence on the response because the electrical time constant is more than 10 times faster than the mechanical.

Table 5.1: Model system's (rotation) motor experimentally verified parameters

Variable	Description	Value	Units
J	rotor inertia	$3.9e^{-4}$	oz-in-s^2
R	armature resistance	8.5	Ohms
L	inductance	$6.17e^{-3}$	H
K_t	torque constant	5.5984	(oz-in)
K_b	back emf constant	.03953	(V-s)/rad
D_1	viscous damping	1.07927e-4	(oz-in)/(rad/s)
K_D	damping constant	.0260	(oz-in)/(rad/s)
T_C	Coulomb friction	.56	oz-in
T_s	static friction	1.5811	oz-in
V_{ref}	rated voltage	24	volts
I_s	break-out current	.2824	amps
I_P	peak current	2.88	amps
N_T	gear ratio	1916.7:1	none

τ_m	mechanical time constant	15.0	ms
τ_e	electrical time constant	.7258	ms
p_1	$1/\tau_m$	68.1351	Hz
p_2	$1/\tau_e$	1377.6	Hz
Kc_r	rotational angle sensor gain	.26	rad/v

Table 5.2: Model system's (translation) motor experimentally verified parameters

Variable	Description	Value	Units
J	rotor inertia	$3.9e^{-4}$	oz-in-s^2
R	armature resistance	8.4	Ohms
L	inductance	$6.17e^{-3}$	H
K_t	torque constant	5.6224	(oz-in)/A
K_b	back emf constant	.0397	(V-s)/rad
D_1	viscous damping	1.07927e-4	(oz-in)/(rad/s)
K_D	damping constant	.0266	(oz-in)/(rad/s)
T_C	Coulomb friction	.5376	oz-in
T_s	static friction	1.4667	oz-in
V_{ref}	rated voltage	24	volts
I_s	break-out current	.2609	amps
I_P	peak current	2.88	amps
N_T	gear ratio (translation link)	127.78:1	none
τ_m	mechanical time constant	14.7	ms
τ_e	electrical time constant	.73452	ms
p_1	$1/\tau_m$	66.7581	Hz
p_2	$1/\tau_e$	1361.4	Hz
Kc_t	translation sensor gain	.7591	in./v

5.4.3 Model System Motor-ID

Unlike the model's motor parameters, the prototype's motor data had a large degree of uncertainty associated with it. The parameters T_C , T_s , and J were omitted and R, K_t, and K_b had been generalized for several frame sizes.

The identification procedure began by determining the armature resistance R. This was performed by measuring resistance across the motor's terminal leads. Several measurements were taken at different shaft orientations and averaged. The inertia term, J was determined using the method suggested in Electro-Craft (1980). This procedure was conducted by removing the armature from the test motor and connecting it to a 3 foot, .02 inch diameter wire. The armature was freely suspended from the cable so that it could oscillate uninhibited. A half twist was applied to the suspended armature, and the time that it reached 20 oscillations was recorded as t_{test}. The test armature, J_{test} was replaced with an armature of know inertia and the procedure was repeated. The armature inertia under test was then calculated from:

$$J_{test} = J_k \left(\frac{t_{test}}{t_k} \right)^2 \tag{5.6}$$

where J_k was the known inertia and t_k was the time recorded for 20 oscillations of J_k.

K_t, was directly established from K_b (Electro-craft, 1980) through the relationship:

$$K_t = 141.623 \cdot K_b \qquad \text{[oz-in/A; V/rad/sec]} \tag{5.7}$$

where the coefficient term represents a unit conversion. K_b was estimated from the electrical equation of the motor that neglects inductance and operates under a no load condition, or:

$$K_b = \left(\frac{V - IR}{\omega} \right) \tag{5.8}$$

(Note that measuring current, I, which represents torque losses, and the applied voltage, V are easily accomplished for any step response. Speed, ω, is also easily determined by taking the derivative of the position response.)

By stepping both the rotational and translational prototype motors with inputs of 3,4,5, and 10 volts, the parameters needed to compute (5.7) and (5.8) were determined. Figures 5.8 and 5.9 show the responses.

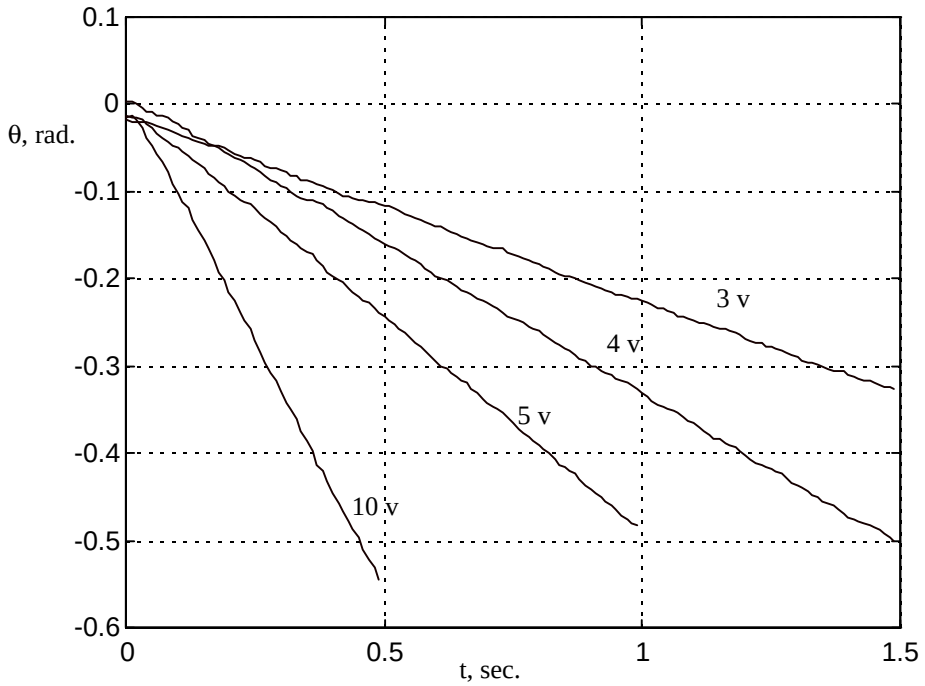

Figure 5.8: Prototype rotation motor response for [3,4,5,10V] steps

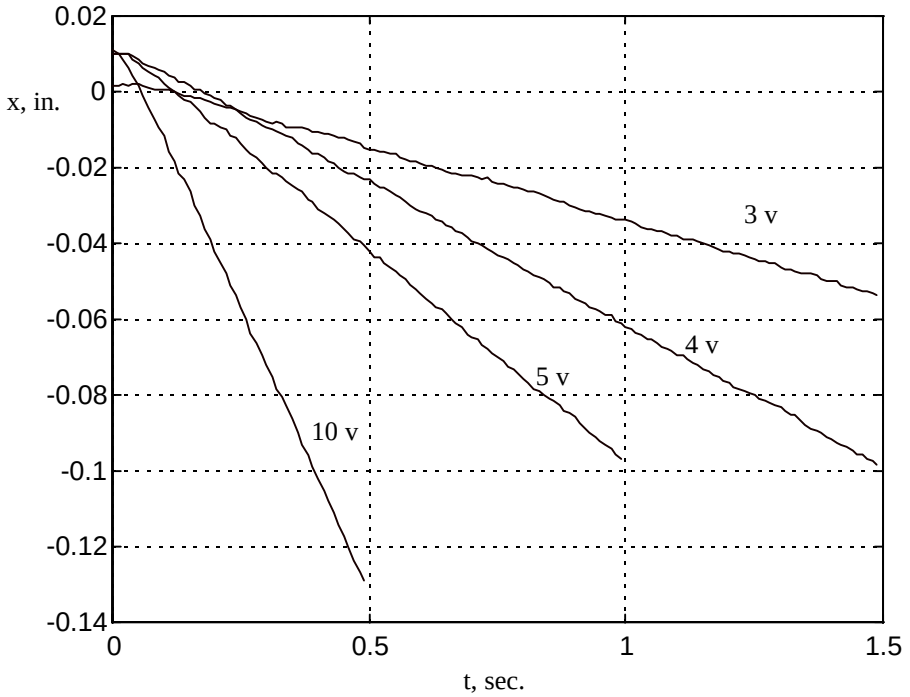

Figure 5.9: Prototype translation motor response for [3,4,5,10V] steps

Notice that stiction was more pronounced for the lower voltage step inputs. Plastic, non-bearing, cheaply made gears account for the often high and unpredictable stiction effects at these lower velocities. The motor velocities for these different step inputs were determined by taking the slope of the response at steady state and dividing it by N_T for the rotational motor and $N_T r$ for the translational motor. The gear ratio was determined by opening the gear box and counting the teeth for each stage. Steady state current and voltage were measured for each run. With these terms established, K_b was calculated for each response and then averaged for the respective motors. Once K_b was established, K_t was computed.

To test the parameters, a step input voltage was applied to each prototype motor that was just above break-out voltage. Speed was determined from this response by using the Matlab function polyfit. The slope from this calculation was the shaft velocity. Coulomb torque was then solved using equation (3.29) where it was assumed that acceleration, damping and load terms were set to zero. This is a fair assumption because measurements were taken after steady state had been reached at the lowest possible sustainable speed. The equation used to determine T_C was:

$$T_C = \frac{K_t}{R}\left(V_{test} - K_{b_{avg}}\omega_{test}\right) \tag{5.9}$$

Static friction, T_s, was again determined using equation (5.5).

The estimated parameters were substituted into equation (5.3). Figure 5.10 shows the experimental and analytical responses of the prototype system's rotation motor to a 2.42 volt step input. Figure 5.11 shows the translational response to a 2.6 volt step input. Both closed form responses show excellent agreement with the experimental responses and suggest that the motor parameters are correct.

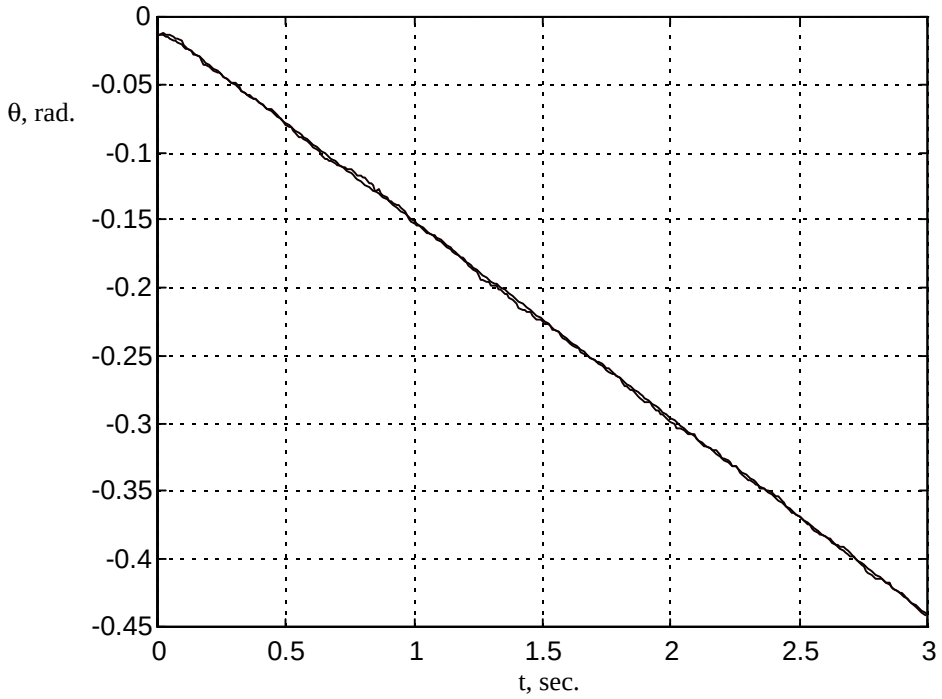

Figure 5.10: Prototype rotation motor position response
closed form solution vs. experimental

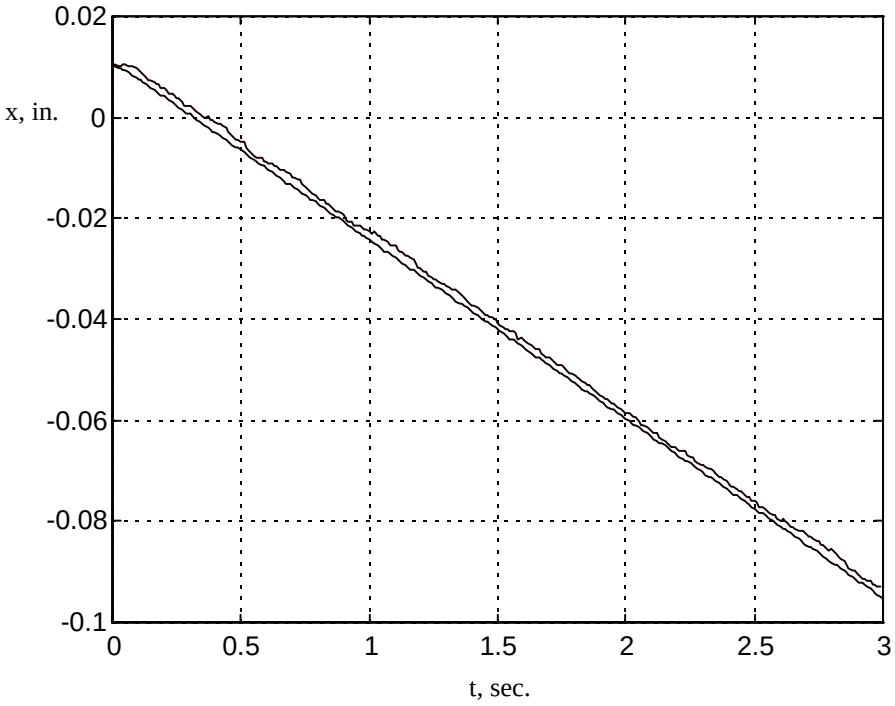

Figure 5.11: Prototype translation motor position response
closed form solution vs. experimental

The analytical response from equation (5.4), which includes static and viscous friction terms, more closely matches the experimental responses for this test. Figure 5.12 illustrates this point.

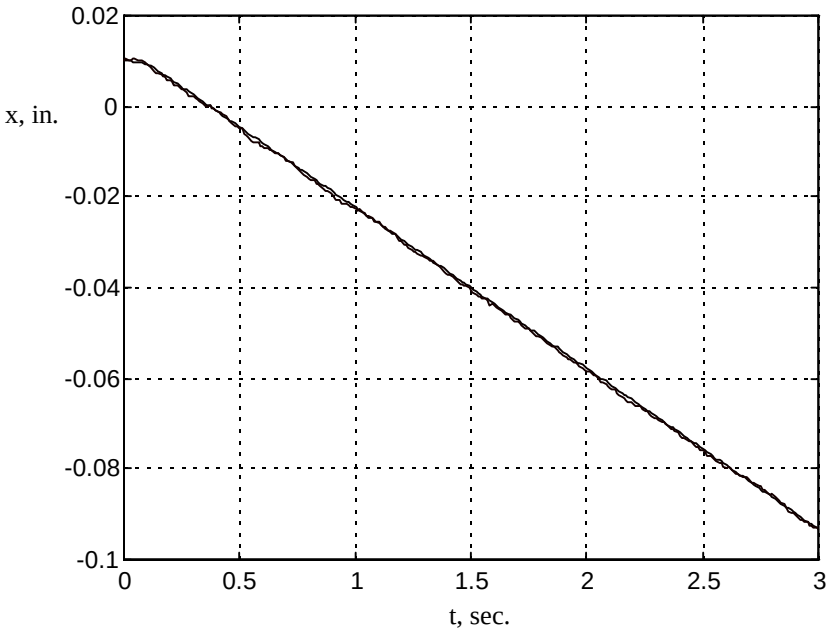

Figure 5.12: Prototype translation motor position response;
analytical with modeled stiction vs. experimental

Figure 5.13 highlights the stiction effect in Figure 5.12. From this exploded view, it can be concluded that the simple cut-off function in equation (5.4) closely modeled the stiction phenomenon. The cut-off time constant, t_s, in equation (5.4), was found to be .08 seconds. This represents the length of time that the stiction pulse was on.

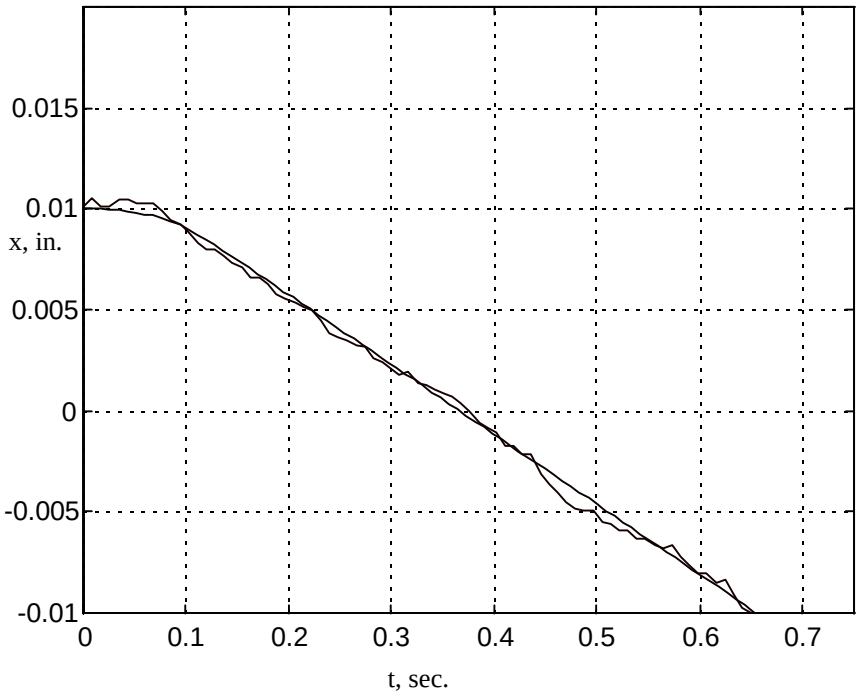

Figure 5.13: Exploded view of Figure 5.12; highlighting stiction

Viscous damping was also manually adjusted in equation (5.4). The analytical response in Figure 5.12 is for a damping term equal to 1.0e-5 (oz-in)/(rad/s) which is very close to zero

Tables 5.3 and 5.4 list the experimentally determined motor parameters for the prototype system. The inductance term was not supplied by the manufacturer and was omitted from the testing. Figure 5.13 illustrates that setting inductance to zero for this system is a reasonable assumption. Furthermore, the influence of the electrical time constant is not discernible for this position response because of the high level of stiction.

Table 5.3: Prototype system's (rotation) motor experimentally verified parameters

Variable	Description	Value	Units
J	rotor inertia	$8.3711e^{-5}$	oz-in-s^2
R	armature resistance	23.25	Ohms
L	inductance	(not measured)	
K_t	torque constant	2.8466	(oz-in)/A
K_b	back emf constant	.0201	(V-s)/rad

D_1	viscous damping	1.0e-5	(oz-in)/(rad/s)
K_D	damping constant	.002461	(oz-in)/(rad/s)
T_C	Coulomb friction	.1407	oz-in
T_s	static friction	.1850	oz-in
V_{ref}	rated voltage	24	volts
I_P	peak current	.915	amps
I_s	break-out current	.078	amps
τ_m	mechanical time constant	34.0	ms
p_1	$1/\tau_m$	29.3982	Hz
N_T	gear ratio	420.3	none
Kc_r	rotation angle sensor gain	.2301	rad/v

Table 5.4: Prototype system's (translation) motor experimentally verified parameters

Variable	Description	Value	Units
J	rotor inertia	$8.3711e^{-5}$	oz-in- s^2
R	armature resistance	23.25	Ohms
L	inductance	(not measured)	
K_t	torque constant	3.0736	(oz-in)/A
K_b	back emf constant	0.0217	(V-s)/rad
D_1	viscous damping	1.0e-5	(oz-in)/(rad/s)
K_D	damping constant	.002868	(oz-in)/(rad/s)
T_C	Coulomb friction	.2370	oz-in
T_s	static friction	.3319	oz-in
V_{ref}	rated voltage	24	volts
I_s	break-out current	.108	amps
I_C	running losses current	.078	amps
τ_m	mechanical time constant	29.2	ms
p_1	$1/\tau_m$	34.2728	Hz
N_T	gear ratio	420.3	none
r	equivalent radius	.334645	in.
Kc_t	translation sensor gain	.0655	in./v

The values in Table 5.2 and 5.3 have a degree of uncertainty that were not quantified. Position responses were sensed from inexpensive potentiometers which were calibrated by hand. Because of this, there are most likely small errors in the sensor gains which in turn affects all of the speed related terms such as back emf and the torque constant.

In addition, there are discrepancies in the torque friction terms presented in Tables 5.3 and 5.4 which were measured with the motors coupled to the mechanism. The motors had also been tested unmounted and uncoupled from the mechanical system. Although not identical, most of the motor parameters were found to be in close agreement. However, when the motors were coupled to the mechanical links, misalignment of the transmission shafts probably induced side loads in the nonbearing gearbox. As a consequence, friction terms increased. This was more

pronounced in the translational motor. To simplify the problem and for reasons of expediency, all internal motor, gearbox, and shaft torque frictions were taken to be one composite term for each motor. Measurement uncertainty was one of the reasons why this condition was assumed.

Although the system identification scheme outlined in this section is certainly deficient as discussed, it is more than adequate for proving the legitimacy of the scaling laws put forward in this thesis. The next section will illustrate this point. Future work, however, would be enhanced by using motors with encoders or tachometers and by using traditional system identification methods based on frequency analysis. To be completely accurate, parameters should be identified independently using the methods suggested in Electro-Craft (1980).

5.5 Presentation of Results for Controlled Model and Prototype Systems

The results presented in this section are from the experimental runs of the full model and prototype systems controlled by the algorithm presented in Section 4.2. Appendix F presents the C code that was used to control both systems.

Consider the experimental results of the model system. As in section 4.2, the setpoint is (x=1, y=1 in.) in the local coordinate system. This corresponds to a rotational displacement of .1454 radians and a translational displacement of .9272 inches in the global coordinate system. Figure 5.14 shows the simulated position feedback signal compared to the experimental signal for the model's rotation link. Figure 5.15 shows the analogous signals for the translation link.

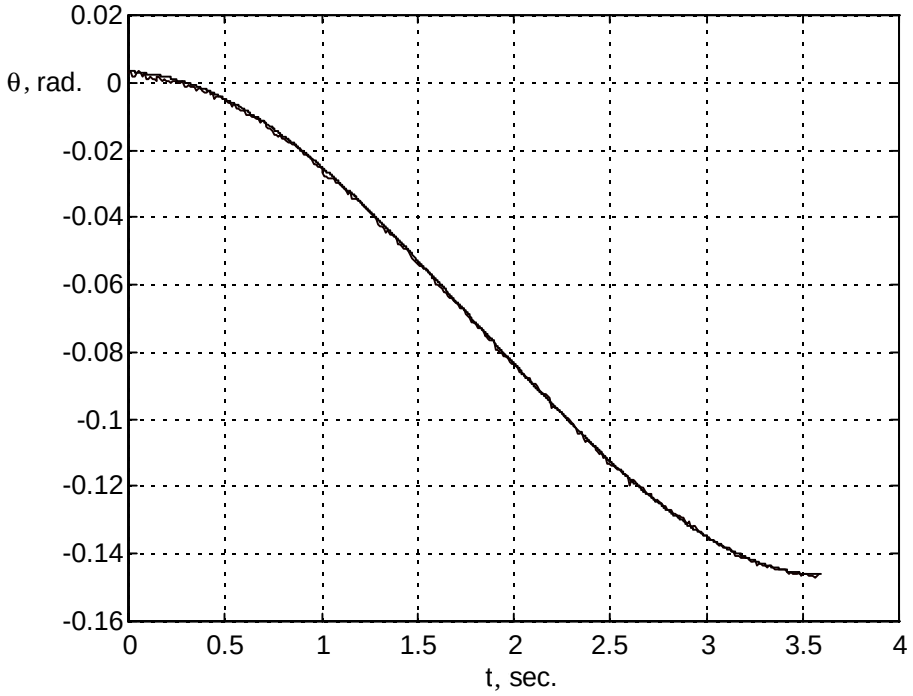

Figure 5.14: Model's rotation link, simulation vs. experimental

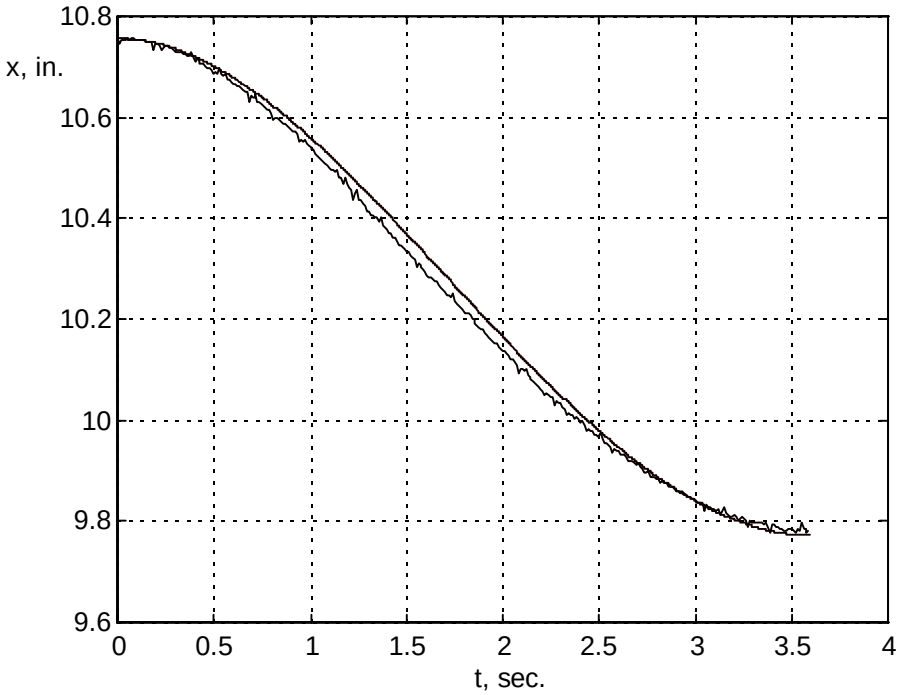

Figure 5.15: Model's translational link, simulation vs. experimental

Both figures reveal excellent agreement between the simulated and experimental runs. In fact, the position errors are only .0012 in. for the rotational link and .0067 in. for the translational link. The position signals are unfiltered and signal noise may have slightly skewed these results. Errors may also be attributable to sensor calibration error, an out-of-round pulley, or slight discrepancies in the translation link's motor parameters.

The small position errors as seen in Figures 5.14 and 5.15 confirm the viability of the computed torque control algorithm for this application. To emphasis the effects of friction compensation, the run is repeated with Static + Coulomb + viscous friction terms set to zero in the control law. Figures 5.16 and 5.17 offer the results for this testing. In general, the links break-out much later and stick earlier when friction compensation is not applied.

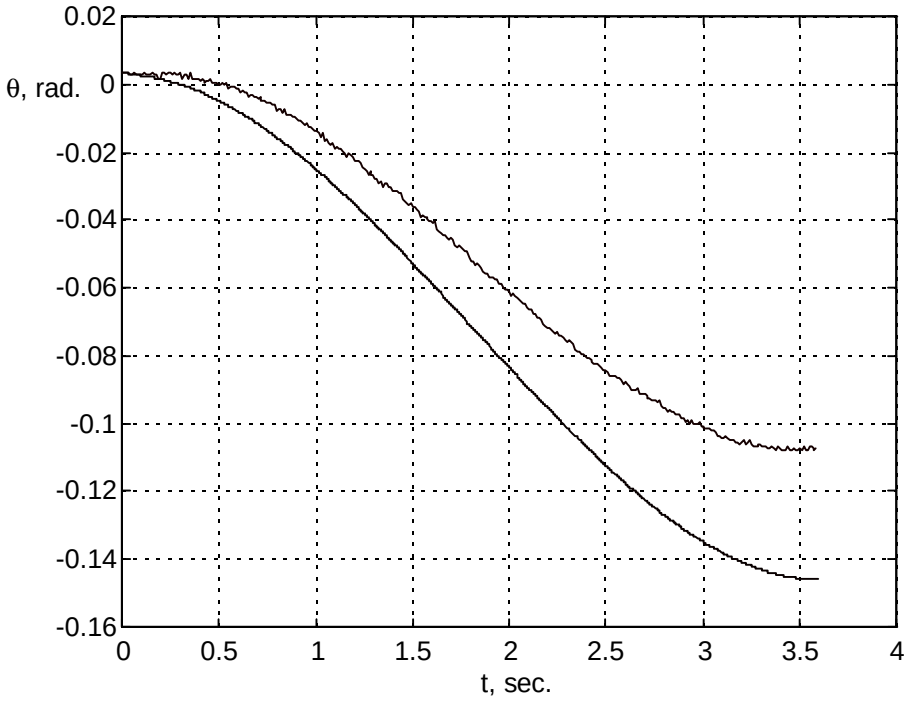

Figure 5.16: Model's rotation link, no friction compensation

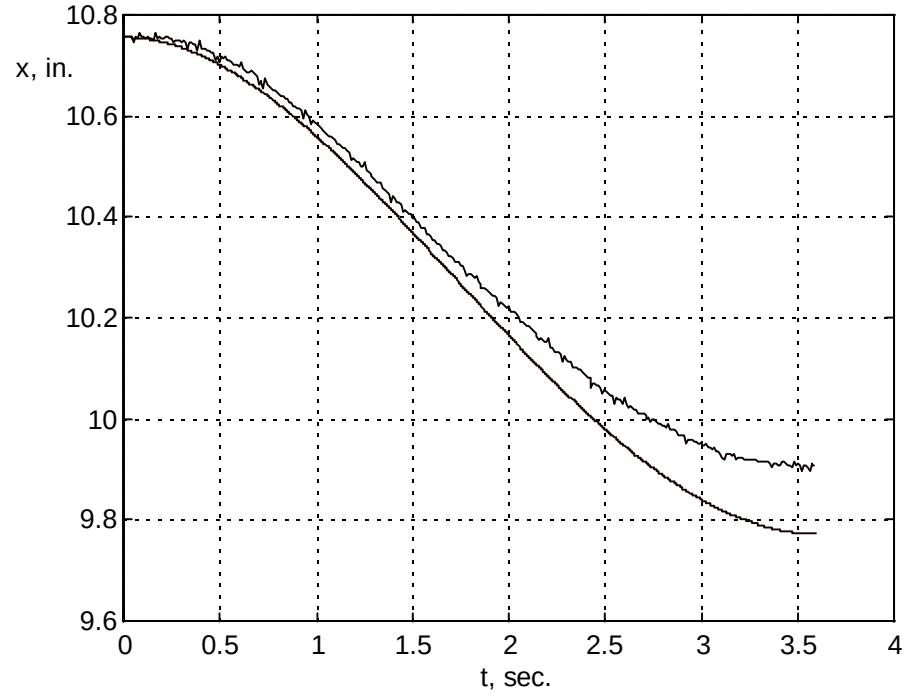

Figure 5.17: Model's translation link, no friction compensation

Figure 5.18 shows the control command with no friction compensation and the position feedback signal for the rotation link. Both signals are shown in terms of volts. For this run, the rotation link did not move until the reference voltage had exceeded 2.5 volts, and it became stuck when the reference voltage fell below 2.5 volts.

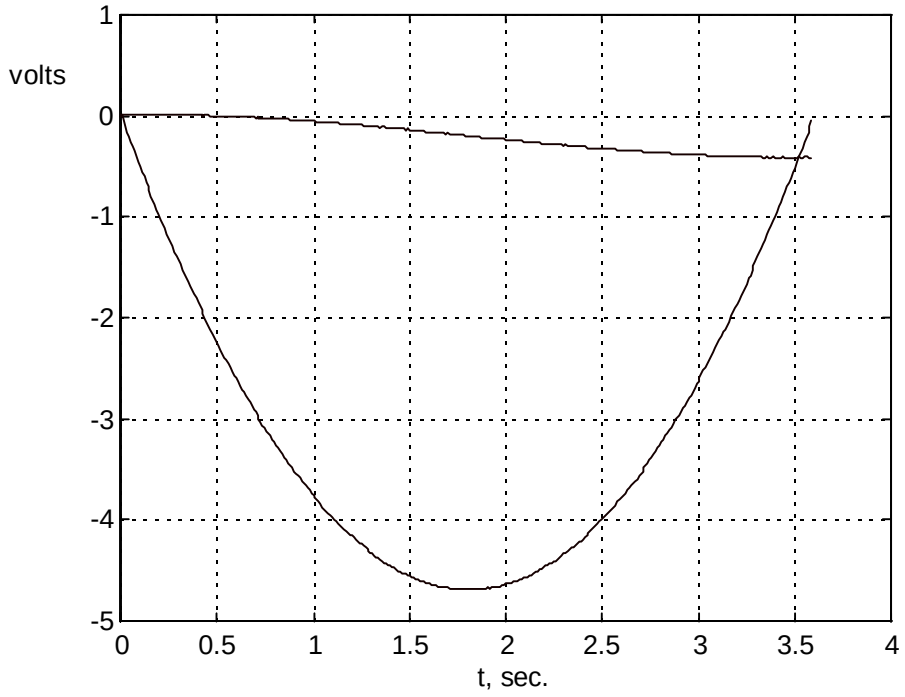

Figure 5.18: Model's rotation link, position
feedback vs. control command, no friction compensation

Figure 5.19 repeats the run that produced Figure 5.18 with friction compensation applied. Observe that static friction compensation produces a pulse at the beginning of the control command signal, while Coulomb compensation adds the voltage equivalent of T_C to the entire control command. Because viscous damping is so small, its compensation effects are not perceptible in this plot.

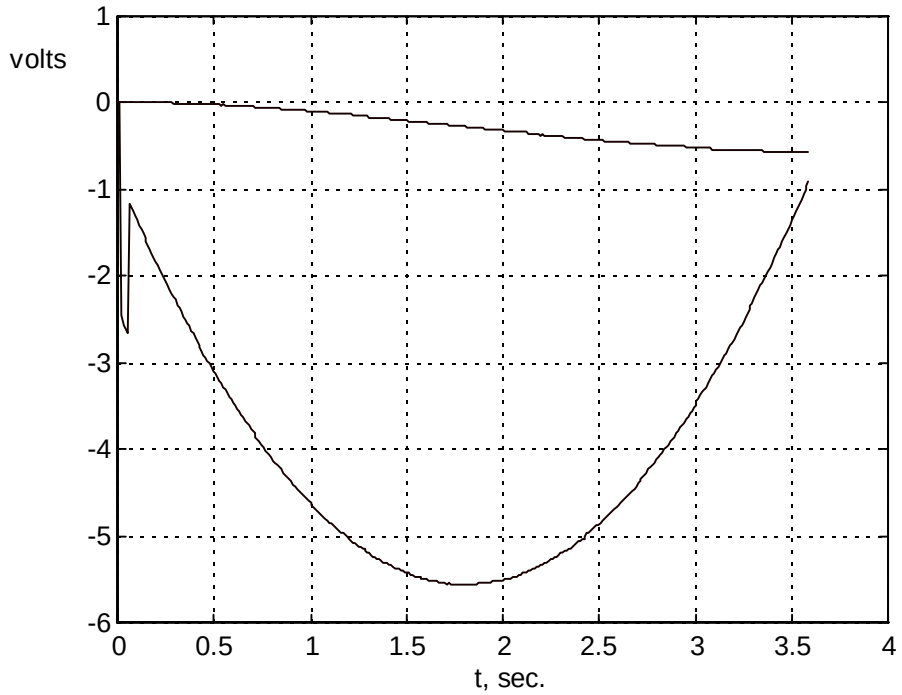

Figure 5.19: Model's rotation link, position
feedback vs. control command, with friction compensation

Now consider producing the above results for the prototype system. As previously discussed, the task is accomplished by scaling the trajectory planner and the gearmotors. The trajectory planner is automatically scaled by entering the prototypes link lengths and desired setpoints as stated in equation (3.22) and simulated in section 4.4. Recall that the prototype's position setpoints are x=.1378 inches and y=.1378 inches in the local coordinate system. From these setpoints, the trajectory planner produces a rotational displacement of .0779 radians and translational displacement of .1324 inches in the global coordinate system.

The Pi terms as derived in section 3.4 can predict whether or not the proposed prototype motors and their parameters listed in tables 5.3 and 5.4 are viable. First consider matching the rotational link motors using the third Pi term and the equation:

$$\theta_g = N_T \theta \tag{5.10}$$

then

$$\Pi_3 = \left[\frac{\theta_g}{N_T \omega_{NL} \tau_m} \right]_{\text{model}} = \left[\frac{\theta_g}{N_T \omega_{NL} \tau_m} \right]_{\text{prototype}} \tag{5.11}$$

The goal is to solve for a reference voltage in the prototype system in order to approximate its stall torque. Equation (5.11) becomes:

$$V_{ref\ p} = \left[\frac{\theta_g}{N_T \frac{1}{K_b} \tau_m} \right]_{\text{prototype}} \cdot \left[\frac{N_T \frac{V_{ref}}{K_b} \tau_m}{\theta_g} \right]_{\text{model}} \tag{5.12}$$

If the peak voltage in Figure 5.15 is used as an estimate for the model's reference voltage V_{ref}, for its rotation motor, then an estimate of the required reference voltage for the prototype's rotation motor is:

$$V_{ref\ p} = \left[\frac{.0779}{420.3 \cdot \frac{1}{.0201} \cdot .0340} \right]_{\text{prototype}} \cdot \left[\frac{1916.7 \frac{4.5879}{.03953} .015}{.1454} \right]_{\text{model}} = .1207 \tag{5.13}$$

Equation (5.13)'s results are suspiciously low. Before proceeding with the calculations of the remaining Pi terms, the prototype's dimensionless friction terms are immediately checked. Using the result from (5.13), the prototype's rotational stall torque is calculated to be:

$$T_{gs_p} = \frac{V_{ref_p} K_{t_p}}{R_p} = .0148 \tag{5.14}$$

This produces prototype dimensionless friction terms of:

$$\begin{aligned} \overline{T}_s &= 12.5195 \\ \overline{T}_C &= 9.5216 \end{aligned} \tag{5.15}$$

The third Pi term together with the results from (5.14) and (5.15) immediately inform the designer that the candidate prototype rotational gearmotor is not a suitable match. If no friction compensation is applied, Coulomb friction torque is more than 9.5 times the motor's stall torque for the calculated reference voltage. The stiction term is more than 12.5 times greater than the stall torque. Simply stated, the reference that produces the desired trajectory path is significantly smaller than the reference that is needed to overcome friction. Theoretically, friction terms in the computed torque controller could cancel the friction effects. However, the ratios in (5.15) indicate that the estimation band is too narrow.

Figure 5.20 shows the position response of the prototype's rotation link with the motor parameters in equation (5.13) used in the controller. Stiction compensation successfully broke the system out, but because it was over estimated, the link was driven beyond its trajectory path. After the stiction pulse was released, the response stuck because Coulomb estimation was under estimated.

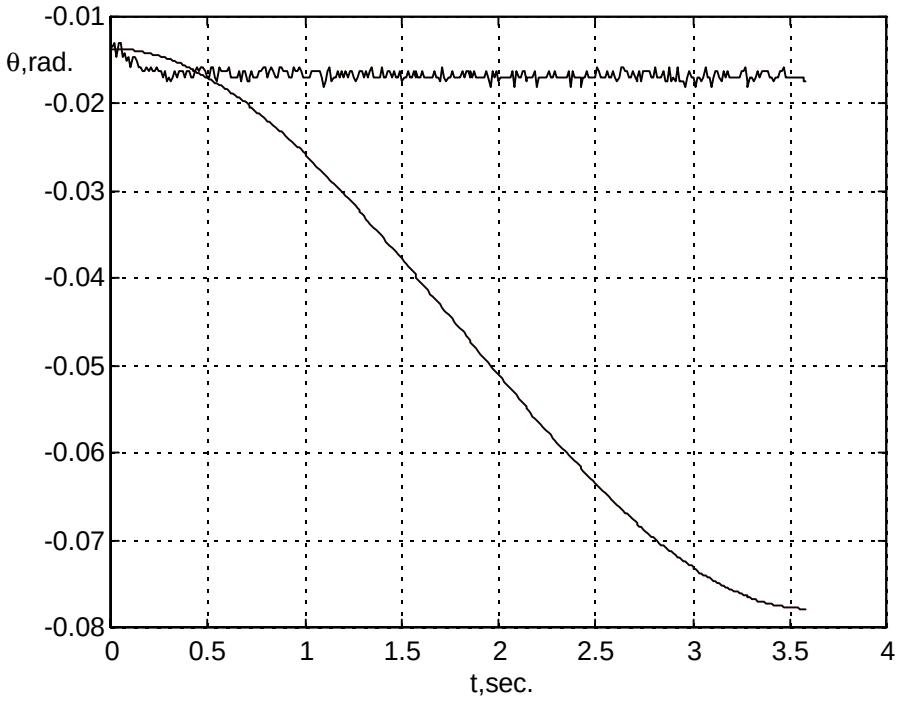

Figure 5.20: Experimental test, prototype rotation link

Figure 5.21 shows the control command reference signal versus the displacement signal for this run. The computed torque controller produced 1.2 volts to compensate for Coulomb friction. This component of the reference command is much greater in magnitude than the component computed to produce the S-curve for the desired trajectory; which had a maximum value of only .1846 volts.

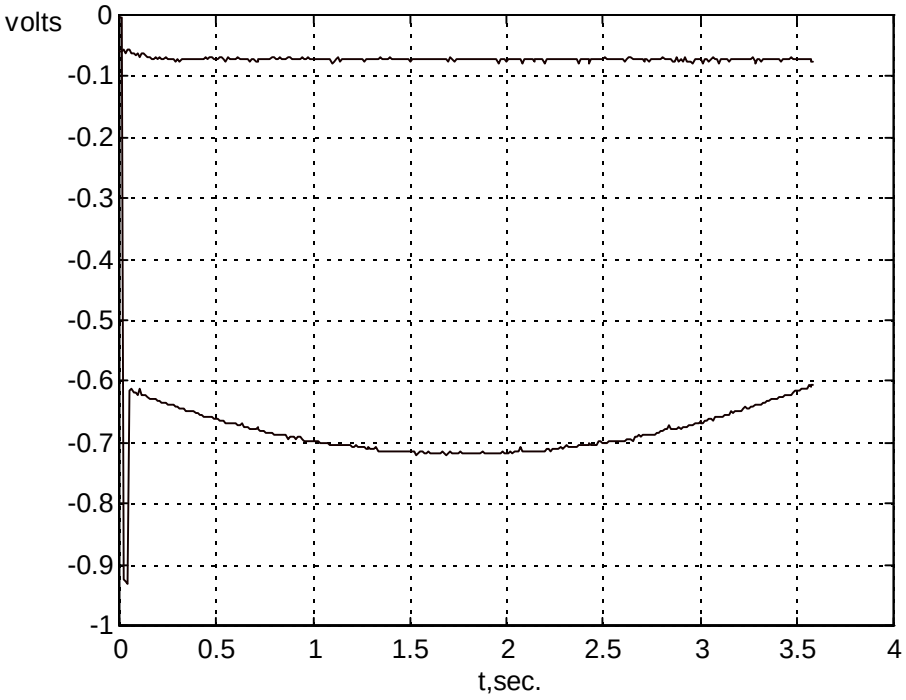

Figure 5.21 Control command signal (1/2 scale)
vs. rotation position signal (full scale)

Figure 5.22 shows the simulated results of a small over estimation of the Coulomb friction term in the computed torque controller. Essentially, the prototype's rotation gearmotor sees this reference as a step input.

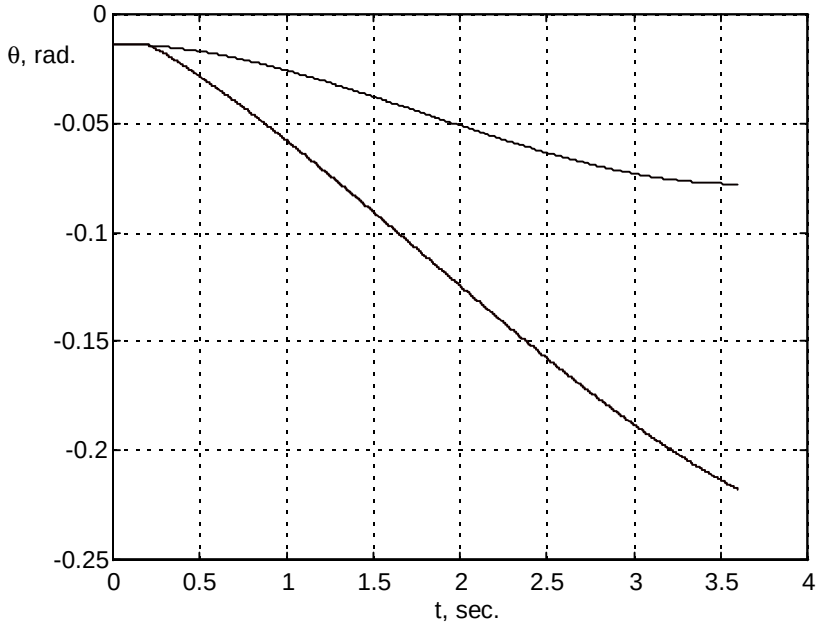

Figure 5.22 Simulation of over estimated Coulomb friction

Figure 5.23 shows the experimental results due to an over estimation of Coulomb friction. For this run, T_C was changed from a value of .1407 oz-in, which was used to generate the response in Figure 5.21 and was the value determined by the system identification scheme, to .19 oz-in which was the minimum value that would sustain a break-out. From the plot, it is clear that Coulomb friction is significantly over estimated, and it is clear from the experimentation that the candidate prototype gearmotor for the rotation link is not a workable solution. The Pi terms predicted this fact.

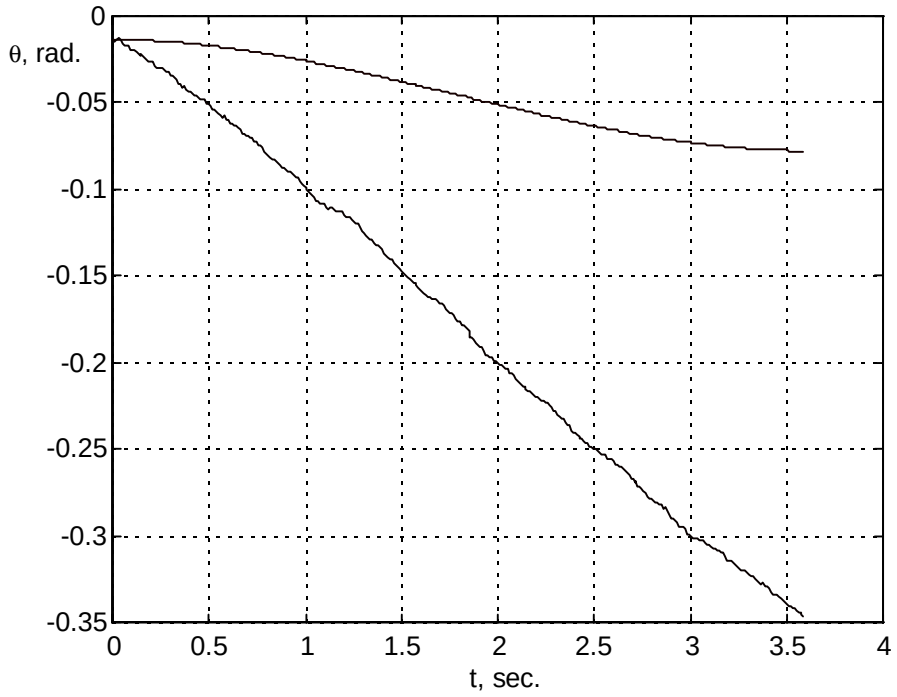

Figure 5.23 Experimentation of over estimated Coulomb friction, prototype rotation link

Figure 5.24 shows the prototype's translation link motion for the experimental run. A slight over estimation of the Coulomb friction term in the controller, necessary to sustain break-out, drove the system too hard and produced a small setpoint error. However, close agreement of the signal shape strongly suggests that the prototype's translational motion did in fact scale successfully to the model's.

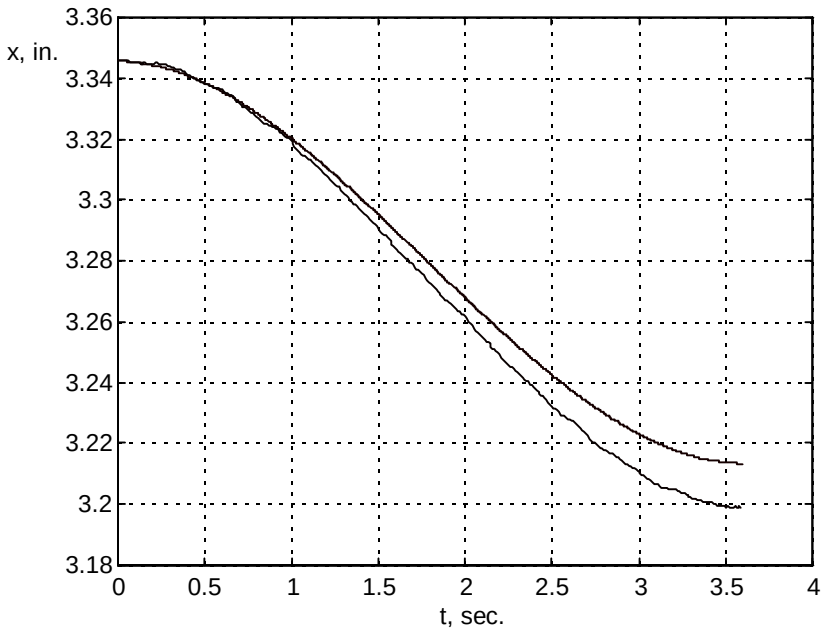

Figure 5.24 Prototype translation link position feedback vs. position reference

Figure 5.25 shows the command reference (1/2 scale) with the position feedback signal for the translational motion. Observe the differences between this plot and Figure 5.21. In Figure 5.21, the command reference is always less in absolute magnitude than the stiction pulse. This means that if the system ever became stuck due to a bad gear tooth or gear irregularity, it would never become unstuck. The translational link control reference in Figure 5.25, however, is greater than the sticking point for more than 70% of the run. If this link became stuck shortly after the stiction pulse, it would remain stuck until time had reached .5 seconds, at which time, the reference magnitude would be greater than the stiction reference.

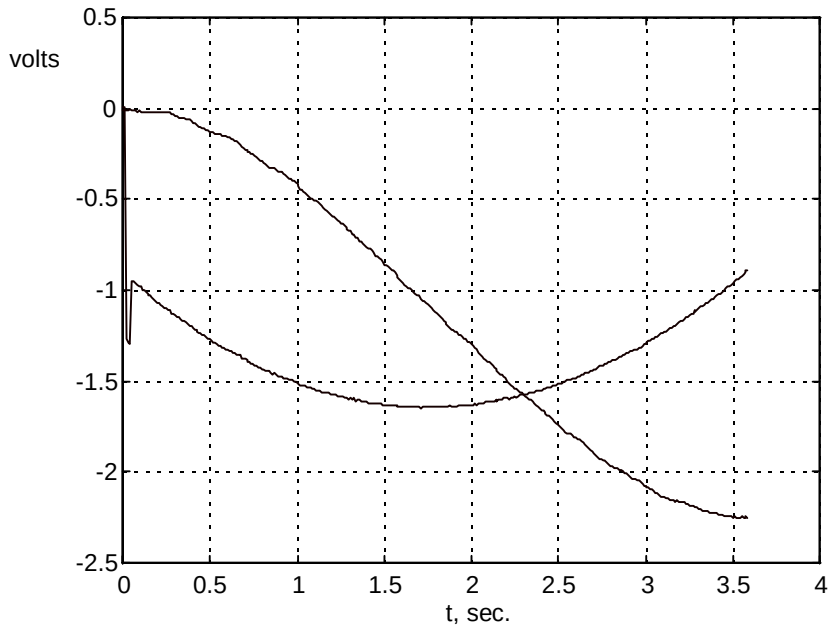

Figure 5.25 Translation control command reference with friction compensation (1/2 scale) vs. position feedback (full scale) in volts

Figure 5.26 repeats the run in Figure 5.25, but with the friction terms set to zero in the controller. The command reference, 1/2 scale in the plot, peaks at an absolute value of 1.4795 volts for this run's initial conditions. (For the prototype's numerical simulation, a zero displacement initial condition produces a reference voltage that peaks at 1.509 volts.) As revealed in this plot, the controller never generates a torque reference greater in magnitude than the stiction torque. Thus the translation link never breaks-out.

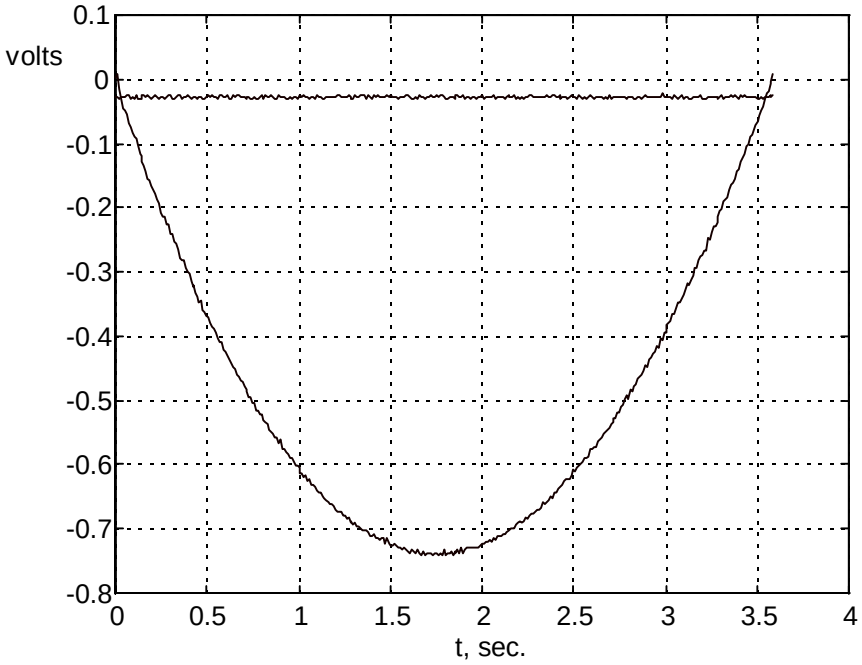

Figure 5.26 Translation control command reference with friction compensation (1/2 scale) vs. position feedback (full scale) in volts

Figure 5.27 repeats the previous plot and shows the scaled experimental position feedback signal versus a simulated feedback response where the friction terms are set to zero.

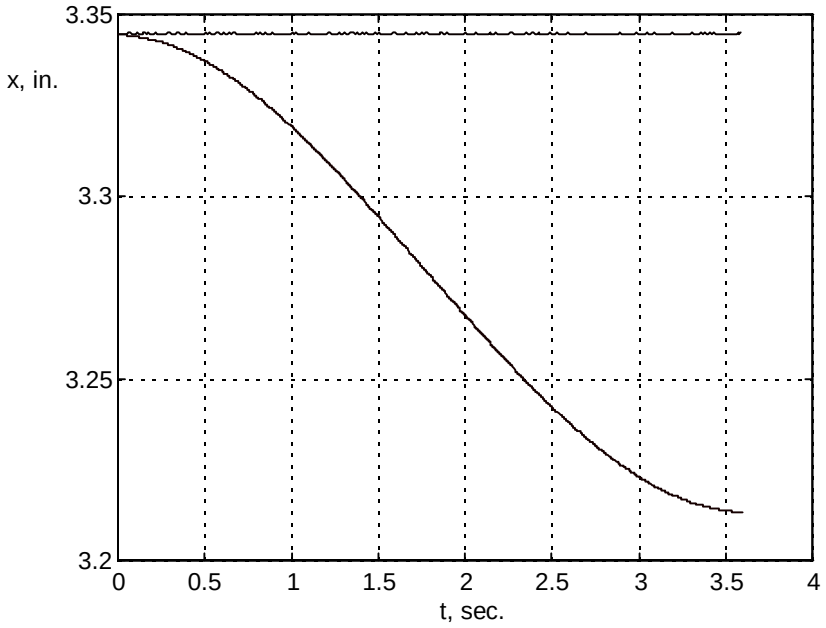

Figure 5.27: Translation link position (experimental) feedback without friction compensation vs. Simulink model with compensation

From Figures 5.24 through 5.27, it is clear that without friction compensation the candidate gear motor for the prototype's translation motion is not viable. Revisiting the Pi terms will shed additional light about the proposed system.

Recall that to achieve similarity between the model and prototype translational motors, that all five previously derived Pi terms need to be satisfied. The experimentation reveals that achieving similarity between the proposed model and prototype systems is impossible without using a controller that provides friction compensation. Π_1 and Π_5 are satisfied in just this way. Friction terms are added in the computed torque controller to cancel the motor's friction effects. The load term in this application is effectively zero so Π_2 is satisfied as well. This leaves satisfying Π_3 and Π_4. Recall that:

$$\Pi_3 = \left[\frac{x}{N_T r \omega_{NL} \tau_m}\right]_{\text{model}} = \left[\frac{x}{N_T r \omega_{NL} \tau_m}\right]_{\text{prototype}} \tag{5.20}$$

and

$$\Pi_4 = \left[\frac{t}{\tau_m}\right]_{\text{model}} = \left[\frac{t}{\tau_m}\right]_{\text{prototype}} \tag{5.21}$$

First consider the third Pi term. If x, N_T , and r are fixed in both the model and prototype systems, then the expression can only be satisfied by adjusting the reference voltage in the no load speed term. The peak voltage applied to the model system that produced the response in Figure 5.11 (less the voltage to compensate for friction) was 8.3274 volts. This value is used in the model's no load speed term in (5.20). To satisfy this Pi term, the reference voltage in the prototype's no load speed term is calculated to be .7589 volts, or:

$$V_{ref_p} = V_{ref_m}\left[\frac{K_{b_p}}{K_{b_m}}\right]\left[\frac{x_p}{x_m}\right]\left[\frac{N_{T_m}}{N_{T_p}}\right]\left[\frac{r_m}{r_p}\right]\left[\frac{\tau_{m_m}}{\tau_{m_p}}\right] = .7597 \tag{5.22}$$

However, the peak voltage for the run that produced Figure 5.26 was 1.4795, nearly twice the value of (5.22). (If zero initial conditions are assumed and the friction terms set to zero, the computed torque controller produces a peak voltage of 1.507 volts.) It appears that equation (5.22) is being incorrectly applied, and to a degree it is. The following analysis will explain the apparent contradiction.

Recall that the third Pi term was originally developed from an uncontrolled step input, however, here it is being asked to predict the peak voltage from a prototype's computed torque controller. Figure 5.28 presents a block diagram of what is being compared.

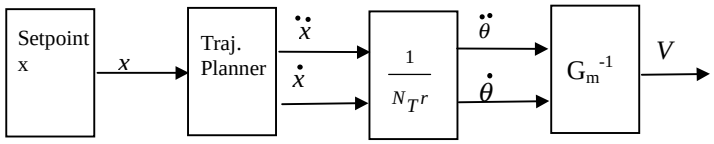

Model System

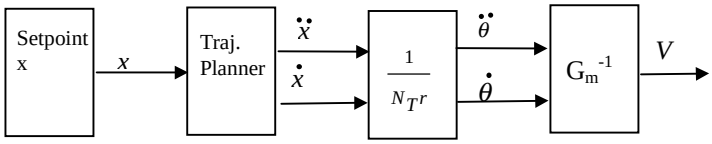

Prototype System

Figure 5.28: Model and prototype voltage references block diagram

If the setpoint *x* in Figure 5.28 is considered to be a step reference, and the trajectory path eliminated, and the model and prototype forward paths are nondimensionalized and set equal, then (5.20) can be rewritten and generalized so that it is applicable to the control scheme under consideration. Bear in mind that the ultimate goal of this exercise is to determine a reference voltage for the prototype gearmotor that can be used to calculate a stall torque which then can be compared to the motor's static and Coulomb torque terms.

First consider the equation of a d.c. motor written without friction terms in the Laplace domain, or:

$$\theta(s) = \frac{V}{K_b\left(s^2\left(\tau_m s + 1\right)\right)}$$

Solving this equation in the time domain produces G_m, or:

$$\theta(t) = \frac{V}{K_b}\left(t + \tau_m\left(e^{\frac{-t}{\tau_m}} - 1\right)\right) \tag{5.23}$$

The inverse analytical model, G_m^{-1} is:

$$V = \frac{K_b \theta(t)}{\left(t + \tau_m \left(e^{\frac{-t}{\tau_m}} - 1 \right) \right)} \tag{5.24}$$

If $\theta(t)$ in equation (5.24) is written in terms of linear displacement as implied in Figure 5.28, then:

$$V = \left(\frac{x}{N_T r} \right) \frac{K_b}{\left(t + \tau_m \left(e^{\frac{-t}{\tau_m}} - 1 \right) \right)} \tag{5.25}$$

The next task is to nondimensionalize this equation so that the model and prototype systems can be compared. This is easily performed by substituting:

$$V = \overline{V} V_{ref} \tag{5.26}$$

then

$$\overline{V} = \left(\frac{x}{N_T r \frac{V_{ref}}{K_b}} \right) \frac{1}{\left(t + \tau_m \left(e^{\frac{-t}{\tau_m}} - 1 \right) \right)} \tag{5.27}$$

Equation (5.27) is nondimensional. If the transients are ignored and time t is set to the final run time, t_f then (5.27) becomes:

$$\overline{V} = \left[\frac{x}{N_T r \frac{V_{ref}}{K_b} \left(t_f - \tau_m \right)} \right] = \left[\frac{x}{N_T r \omega_{NL} \left(t_f - \tau_m \right)} \right] \tag{5.28}$$

Equation (5.28) is a variation on the third Pi term presented in (5.20). If (5.28) is set to unity with:

$$\overline{V} = \frac{V}{V_{ref}} = \left[\frac{V}{V_{peak}} \right]_m = \left[\frac{V}{V_{peak}} \right]_p = 1; \; V = V_{ref} \tag{5.29}$$

then:

$$\left[\frac{x}{N_T r \omega_{NL}\left(t_f - \tau_m\right)}\right]_m = \left[\frac{x}{N_T r \omega_{NL}\left(t_f - \tau_m\right)}\right]_p \tag{5.30}$$

Thus, the prototype's peak voltage for a step input using the same parameters as in (5.22) is:

$$V_{ref_p} = V_{ref_m}\left[\frac{K_{b_p}}{K_{b_m}}\right]\left[\frac{x_p}{x_m}\right]\left[\frac{N_{T_m}}{N_{T_p}}\right]\left[\frac{r_m}{r_p}\right]\left[\frac{t_f - \tau_{m_m}}{t_f - \tau_{m_p}}\right] = 1.51 \tag{5.31}$$

Recall that for this application the final time t_f was set equal for both systems. If the mechanical time constants are significantly smaller than the final run time, then the last ratio in (5.31) approaches unity. This in essence states that for long runs, matching mechanical time constants becomes less important. Using this argument, the fourth Pi term (5.21) is successfully ignored. The simulations and experimental tests confirm this assertion. Both the model and prototype translation links reached the desired setpoints in t_f = 3.6 seconds with small position errors.

The voltage reference of (5.31) matches very closely to the controller's peak voltage for the prototype's translation displacement when friction terms are set to zero (1.51 vs. 1.509 V). Although (5.31) and the experimental testing use two different input functions, the results from this analysis can still be generalized. If a peak voltage $V_{ref,}$ has been calculated for the model system from the analytical equation (5.25), or from the computed torque controller, then a fairly representative estimate of the peak voltage in the prototype system can be calculated from (5.31) given the prototype parameters of K_b, N_T, r, τ_m, and the desired x and t_f references. If the reference voltages are arbitrarily set the same in both the model and the prototype systems, and everything else remains the same, then the prototype's gearing can be quickly computed from:

$$N_{T_p} = N_{T_m}\left[\frac{K_{b_p}}{K_{b_m}}\right]\left[\frac{x_p}{x_m}\right]\left[\frac{V_{ref_m}}{V_{ref_p}}\right]\left[\frac{r_m}{r_p}\right]\left[\frac{t_f - \tau_{m_m}}{t_f - \tau_{m_p}}\right] \tag{5.32}$$

The result from (5.31) is used next to calculate the stall torque term and the dimensionless friction terms for the prototype's translation motor. They are:

$$\begin{aligned} T_{gs} &= \frac{K_t V_{ref}}{R} = .1996 \\ \overline{T_s} &= \frac{T_s}{T_{gs}} = \frac{.3319}{.1996} = 1.6626 \\ \overline{T_C} &= \frac{T_C}{T_{gs}} = \frac{.2370}{.1996} = 1.1873 \end{aligned} \tag{5.33}$$

From (5.33) it is clear that the prototype's peak voltage produces a stall torque that is less than both the static and Coulomb friction terms for the translation motor. As confirmed by the experimental testing, these results clearly predict that the prototype's translational motor will stick if friction compensation is not applied.

As an aside, the analysis in (5.33) could have been forgone if the friction terms had been incorporated in equation (5.25). The closed form solution to the motor equation with static, viscous, and Coulomb friction was solved in Chapter 4 and could have been used as the basis for computing the prototype's peak voltage as just performed. However, this was not pursued in order to keep the analysis simple. The point of this exercise was to determine the prototype's peak voltage from which a stall torque and dimensionless friction terms could be calculated. For the prototype's rotational system, it was immediately clear that the candidate gearmotor was not a workable solution just from attempting to match the original Pi terms. Experimental testing confirmed this prediction. The translation motor had similar friction problems but on a much smaller scale. Because of this, friction compensation was successfully applied.

5.6 Summary

In this chapter, the model and prototype hardware configurations used in the experimental testing were presented and discussed. An overview of the experimental approach for confirming the validity of the Pi terms was treated. An off-line motor parameter identification methodology was presented along with experimentally verified motor constants for the model and prototype systems. Finally, experimental testing was conducted on both the model and prototype systems to verify the simulation results and to validate the Pi based scaling laws. The third Pi term was re-derived using similitude methods from a simplified computed torque controller that omitted friction compensation. This version of the third Pi term facilitated the scaling of the prototype's displacement, voltage, and gearing. It was found to be especially useful for predicting the prototype's peak voltage given a desired step displacement. The peak voltage was in turn used to calculate a stall torque and the dimensionless friction terms. The dissimilar model and prototype translation motors achieved similarity when controlled by a computed torque controller. This controller included friction terms to eliminate the motors' internal friction effects, and used equal t_f values that were significantly longer than the motors' mechanical time constants. The combined effect successfully scaled the translation motion which was experimentally verified. Scaling of the rotation motion failed because the prototype's peak voltage generated from the controller produced a stall torque that was significantly less than the motor's friction terms. Accurately estimating the friction terms for use in the controller was found to be an insurmountable problem.

To summarize, the experimental testing in this chapter suggested that the prototype motors should be selected by first matching as closely as possible the original five Pi terms. If only dissimilar motors are available for use, the prospect of achieving similarity can be quickly predicted by evaluating the modified third Pi term and the dimensionless friction terms that form Π_1 and Π_5.